CO-REGISTRATION OF CHANG'E-1 STEREO IMAGES AND LASER ALTIMETER DATA FOR 3D MAPPING OF LUNAR SURFACE

K. Di *, Z. Yue , M. Peng , Z. Liu

State Key Laboratory of Remote Sensing Science, Institute of Remote Sensing Applications, Chinese Academy of Sciences, P. O. Box 9718, Beijing 100101, China - {kcdi, yuezy, pengman, liuzq}@irsa.ac.cn

Commission IV, WG IV/7

KEY WORDS: Cheng'E-1 orbiter, CCD image, laser altimeter data, co-registration, 3D surface matching

ABSTRACT:

This paper presents a method for co-registration of Chang'E-1 lunar orbiter stereo images and laser altimeter (LAM) data for 3D mapping of lunar surface. First, a digital elevation model (DEM) is automatically generated from the three-line CCD stereo images based on rigorous pushbroom sensor model and multi-level image matching. The DEM is then registered to LAM data through surface matching with a 3D rigid transformation model. Consequently, the exterior orientation parameters of the images are adjusted using the rigid transformation model so that the images and LAM data are co-registered. The experimental results demonstrate that the inconsistency between the CCD images and the LAM data is significantly reduced by this co-registration.

1. INTRODUCTION

China's first lunar probe Chang'E-1 (CE-1) was successfully launched on 24 October 2007 from Xichang Satellite Launch Center. It entered lunar orbit on 5 November and acquired the China's first image of lunar surface on 20 November (Li et al., 2010a). The spacecraft operated until 1 March 2009, when it impacted the surface of the Moon at 08:13 UTC (Du, 2009). The four scientific objectives of the CE-1 mission were: to obtain three-dimensional stereo images of the lunar surface, to determine the distribution of some useful elements and to estimate their abundance, to survey the thickness of lunar soil and to evaluate the resource of ^{3}He, and to explore the environment between the Moon and Earth (Sun et al., 2005)..

CE-1's CCD camera had a full coverage of the Moon and the LAM acquired about 912 millions of laser points. The LAM data has been used to generate a lunar global topographic model and to identify some new terrain features (Ping et al., 2009; Li et al., 2010b). A 1:2.5 million scale global image mosaic has been produced using the CCD images after radiometric and geometric processing, map projection, mosaicking and editing (Li et al., 2010a). In the process, LAM DEM data was used to correct the positional errors of the geometric processing results (Li et al., 2010a). In order to reach the highest potential of lunar surface mapping using the stereo CCD images and the LAM data, a detailed investigation of the co-registration of image and LAM data is desirable.

This paper presents a method for co-registration of Chang'E-1 stereo images and laser altimeter data for 3D high-precision mapping of lunar surface. First, a DEM is automatically generated from the CCD stereo images based on rigorous pushbroom sensor model and multi-level image matching. The DEM is then registered to LAM data through surface matching with a 3D rigid transformation model. Consequently, the exterior orientation parameters (EOPs) of the images are adjusted using the rigid transformation model so that the images and LAM data are co-registered.

The rest of the paper is organized as follows. Section 2 presents the photogrammetric model of CE-1 CCD imagery and the procedure for DEM generation from stereo images. Section 3 briefly describes the approach to calculate LAM elevation data from LAM range measurements. Section 4 presents the method for co-registration of CE-1 CCD image data and LAM data. Section 5 shows the experimental results. Conclusions are given in Section 6.

* Corresponding author.

2. GEOMETRIC MODELING OF CCD IMAGERY AND DEM GENERATION FORM STEREO IMAGES

2.1 Rigorous Geometric Modelling of CE-1 Stereo CCD Imagery

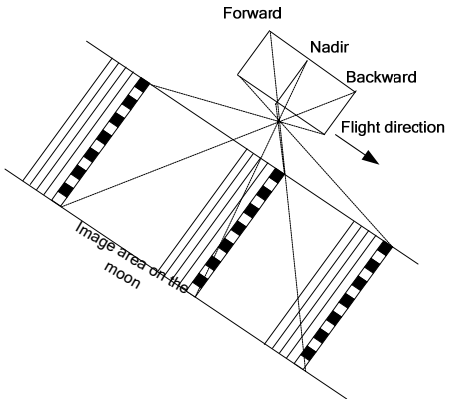

Figure 1. CE-1 stereo camera imaging configuration

The CE-1 CCD camera is a three line pushbroom camera which is implemented on an area array CCD sensor. The CCD array has 1024×1024 pixels, with each pixel being 14 μm ×14 μm in the chip. The forward-, nadir- and backward-looking images of the Moon are generated by reading the 11th, 512th and 1013th rows that are perpendicular to the flight direction (Figure 1). The convergence angle between the adjacent views is 16.7°. At a 200 km altitude, the image spatial resolution is 120 m and the swath width is about 60 km. The focal length of the CCD camera is 23.33 mm.

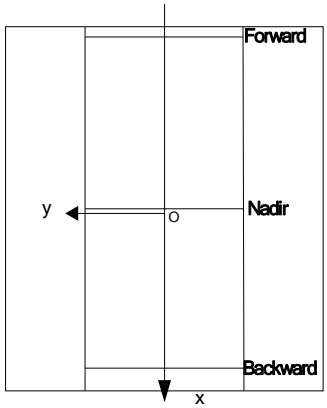

Figure 2. Focal plane frame of the CE-1 CCD

The actual imaging area is 1024 rows by 512 columns. The focal plane frame is shown in Figure 2. The pixel coordinates are transformed to the focal plane frame with the following equations.

$$
\begin{aligned}
x_{backward} &= (x_p - 11) * pixelsize - x_0 \\
x_{nadir} &= (x_p - 512) * pixelsize - x_0 \\
x_{forward} &= (x_p - 1013) * pixelsize - x_0 \\
y_{backward} &= y_{nadir} = y_{forward} = (y_p - col) * pixelsize - y_0
\end{aligned} \tag{1}
$$

where

$x_{forward}$, $y_{forward}$ = focal plane coordinates in forward-looking image

x_{nadir}, y_{nadir} = focal plane coordinates in nadir-looking image

$x_{backward}$, $y_{backward}$ = focal plane coordinates in backward-looking image

x_p, y_p = center position (511.5, 255.5) of the actual imaging area

x_0, y_0 = principle point position in the focal plane frame

pixelsize = size of per pixel in CCD (0.014 mm)

col = pixel position in column direction

It is worth to note that $x_{forward}$, x_{nadir}, and $x_{backward}$ are fixed for all the image lines of forward-, nadir- and backward-looking images respectively due to the pushbroom imaging principle.

In order to transform the focal plane frame to the lunar body-fixed frame (LBF) for topographic mapping, the EOPs of each image line should be obtained by interpolation using the spacecraft's trajectory and pointing vectors. Since the orbit trajectory data are defined in J2000 frame, they are firstly transformed from J2000 to LBF using Equations (2).

$$
\begin{aligned}
R_{IAU}^{INS} &= R_{J2000}^{INS} R_{IAU}^{J2000} \\
A_{IAU} &= A_{J2000} R_{IAU}^{J2000}
\end{aligned} \tag{2}
$$

where R_{IAU}^{INS} = orientation of CCD image in LBF

R_{J2000}^{INS} = orientation of CCD image in J2000

R_{IAU}^{J2000} = rotation matrix from J2000 to LBF

A_{J2000} = position of CCD perspective center in J2000

A_{IAU} = position of CCD perspective center in LBF

Polynomials can be used to model the change of EOPs of the image lines of a pushbroom sensor (Yoon and Shan, 2005; Shan et al., 2005). Here we use third order polynomial to model the EOPs of the CE-1 CCD images.

$$
\begin{aligned}
X(t) &= a_0 + a_1 t + a_2 t^2 + a_3 t^3 \\
Y(t) &= b_0 + b_1 t + b_2 t^2 + b_3 t^3 \\
Z(t) &= c_0 + c_1 t + c_2 t^2 + c_3 t^3 \\
\omega(t) &= d_0 + d_1 t + d_2 t^2 + d_3 t^3 \\
\varphi(t) &= e_0 + e_1 t + e_2 t^2 + e_3 t^3 \\
\kappa(t) &= f_0 + f_1 t + f_2 t^2 + f_3 t^3
\end{aligned} \tag{3}
$$

where $X(t), Y(t), Z(t)$ = position of the perspective center of the sensor at time t

$\omega(t), \varphi(t), \kappa(t)$ = pointing angles at time t

$a_0, \ldots, f_3$ = polynomial coefficients

t = acquisition time of each line

To check the applicability and accuracy of third order polynomials, we examined the trajectory and pointing data of Orbit 562 (acquired between 00:23:32.001 and 00:26:22.00 on Oct 26, 2007). For comparison purposes, we used both second and third order polynomials. The residuals of the trajectory and pointing data are shown in Figure 3, and the root mean square errors (RMSEs) are listed in Table 1.

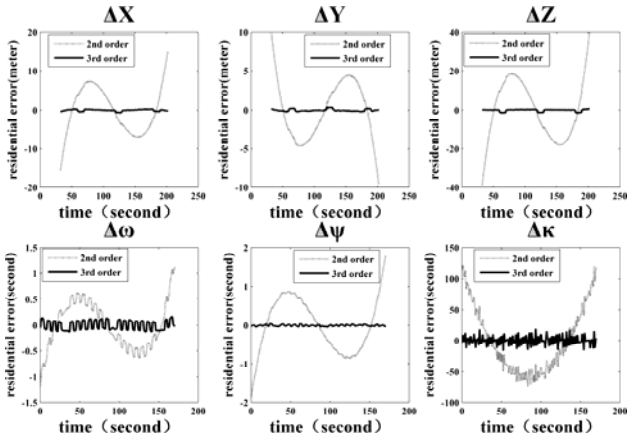

Figure 3. Residuals of polynomial fitting for orbit trajectory and pointing data

Polynomial order	Position (meter)			Orientation (second)		
	X	Y	Z	Ω	φ	K
2	6.03	3.82	15.4	0.45	0.72	53.59
3	0.23	0.14	0.57	0.09	0.02	7.62

Table 1. RMSE of polynomial fitting of EOPs

From the figures and the table, it can be easily observed that third order polynomials are much better than second order polynomials in modelling the EOPs. Thus, third order polynomial is adopted in this research.

After the above geometric modelling process, rigorous collinearity equations are established fro each image line of forward-, nadir- and backward-looking images.

2.2 Multi-level Matching of CE-1 Stereo Images

To produce DEM from CCD stereo images after rigorous modelling, we have developed a multi-level image matching method. The flowchart is shown in Figure 4. Image pre-processing is done using Gaussian filter to remove noises. Interest points are generated by Förstner operator and matched using normalized correlation coefficients.

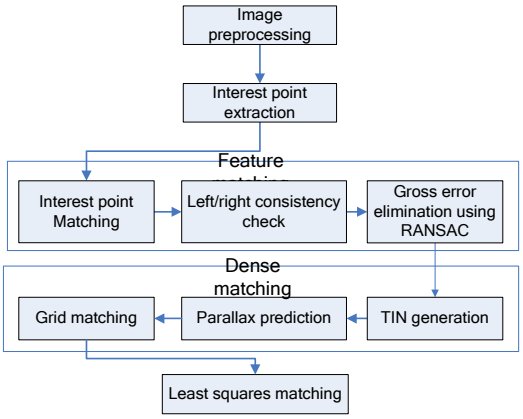

Figure 4. Multi-level stereo image matching

Matching error detection is performed using left/right consistency check. As shown in Figure 5, from left image to right image, P1 matches Q1, and P2 matches Q2; from right image to right image, Q1 matches P1, and Q2 matches P2. Through the left/right consistency check, (P1, Q1) are accepted as correct matches, while (P2, Q2) and (Q2, P3) are discarded as mismatches.

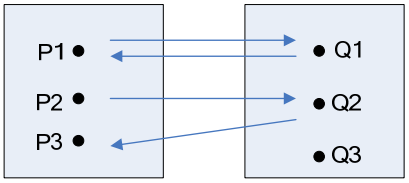

Figure 5. Left/right consistency check

To ensure the reliability of interest point matching, a RANSAC process is applied to further eliminate possible gross errors (mismatches) using a 2D similarity transformation model.

$$\begin{bmatrix} x_r \\ y_r \end{bmatrix} = \begin{bmatrix} a & -b \\ b & a \end{bmatrix} \begin{bmatrix} x_l \\ y_l \end{bmatrix} + \begin{bmatrix} c \\ d \end{bmatrix} \quad (4)$$

where

x_l, y_l = image coordinates of left (forward-looking) image

x_r, y_r = image coordinates of right (backward-looking) image

a,b,c,d = transformation coefficients

After matching of interest points, a triangulated irregular network (TIN)-controlled dense image matching method (Li et al., 2007) is adopted for dense grid matching of CE-1 stereo images. Firstly, a TIN is generated from the matched interest points on the left image, and the x- and y- parallaxes are calculated at each vertex. Second, a grid of 3×3 pixels is generated in the left image and the homologous image point of each grid point on the right image is predicted using linear interpolation of parallaxes from vertices of the triangle that covers the grid point. The actual homologous point in the right

image is determined by cross correlation within a small search range from the predicted position. At last, least squares matching method is applied to reach sub-pixel accuracy.

After image matching, 3D positions of the matched points are calculated using space intersection with the collinearity equations. The final DEM was generated using Kriging interpolation.

3. PROCESSING OF LAM DATA

Using 1064 nm laser wavelength, CE-1's LAM has a 200 meter footprint and 5 meter ranging resolution. The along-track point spacing is 1.4 km and the cross-track spacing is about 7 km at the equator. Overall, more than 1000 orbits of LAM data with a total of 9,120,000 points covering the entire lunar surface were obtained.

Figure 6 shows a diagram of LAM ranging and elevation calculation (Ping et al., 2009). In the figure, u is a laser altimeter measuring vector at a certain measuring time, which is determined by the altimetry ranging and its corresponding attitude; R_S is the selenocentric position vector of the satellite, which is derived from spacecraft trajectory; R is the mean radius of the Moon. The selenocentric position vector R_G of the light spot can be computed by combining u and R_S; subsequently, the elevation h of the light spot can be calculated by referencing R_G to the datum R.

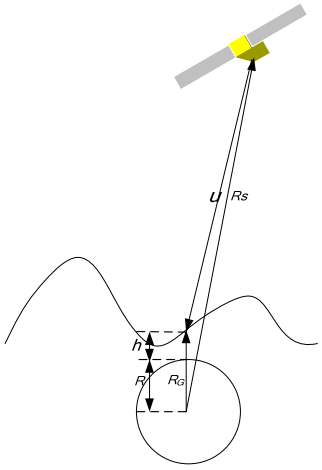

Figure 6. A diagram of LAM ranging and elevation calculation

4. CO-REGISTRATION OF CCD IMAGE DATA AND LAM DATA

4.1 Co-registration based on 3D Surface Matching

The purpose of CCD and LAM data co-registration is to reduce the inconsistency between the two datasets so that to achieve a higher mapping accuracy. As a result, the accuracy of the EOPs of the CCD images can be improved using the LAM data as ground control.

We use the iterative closest point (ICP) algorithm (Besl and McKay, 1992) for registration of DEM to LAM point cloud. As represented in Equation (5), the goal of the ICP algorithm is to minimize the sum of square errors with respect to the CCD DEM points and the corresponding closest LAM points. In order to stabilize the ICP solution, a LAM DEM is generated from the LAM point cloud by Kriging interpolation. In each iteration step, the algorithm selects the closest points as the correspondences and re-calculates the rotation and translation parameters (R, t) of the rigid transformation to minimize the equation

$$\mathrm{F} = \min_{R,t} \sum_{i=1}^{N_m} \sum_{j=1}^{N_d} \left\| m_i - (R d_j + t) \right\|^2 \qquad (5)$$

where m_i =coordinates of the LAM DEM points

d_i = coordinates of the CCD DEM points

t = a 3×1 vector that describes the translations between the two datasets

R = a 3×3 matrix that describes the rotations between the two datasets

The procedure of the ICP algorithm is as follows.

Step 1. Initialize the rotation matrix R as a unit matrix and translation vector as 0.

Step 2. Search the closest point pairs between the CCD DEM and the LAM DEM. Suppose there are N pairs of points found.

Step 3. The coordinates of the point pairs in the two datasets are centralized using Equation (6) in order for stabilization of the solution.

$$m_i' = m_i - \frac{1}{N} \sum_{i=1}^{N} m_i \qquad (6)$$

$$d_i' = d_i - \frac{1}{N} \sum_{i=1}^{N} d_i$$

Step 4. Find R_1 to minimize F' by a SVD based method (Arun et al., 1987); calculate t_1 with Equation (8).

$$\mathrm{F}' = \min_{R_1} \sum_{i=1}^{N} \left\| m_i' - R_1 * d_i' \right\|^2 \quad (7) \quad t_1 = \frac{1}{N} \sum_{i=1}^{N} m_i - R_1 \frac{1}{N} \sum_{i=1}^{N} d_i \qquad (8)$$

Step 5. Use equation 9 to update (R, t).

$$R = R_1 * R$$
$$t = R_1 * t + t_1 \qquad (9)$$

Step 6. Use (R, t) to update the CCD DEM points.

$$d_i = R d_i + t \qquad (10)$$

Step 7. Repeat Steps 2 to 6 until the termination condition is met, i.e., the change of the minimum distance (F') between two successive iterations is less than a threshold.

After the convergence of the ICP algorithm, the resultant (R, t) parameters are applied the EOPs of the images so that the

subsequent photogrammetric measurement from the stereo images will be of higher accuracy, i.e., more consistent with the LAM data.

4.2 Co-registration by Projecting LAM Points onto CCD Images

Another method to register the LAM points and the CCD images is to project the LAM points onto the images through collinearity equations. If the CCD images and the LAM data are perfectly consistent, the projected positions on the forward-, nadir- and backward-looking images will be homologous points. Differences of the projected points from the actual homologous points reflect the co-registration errors between the two datasets.

Sine the EOPs of each image scan line vary, we have to search the best scan line (for each LAM points) so that we can use its EOPs to project the LAM point onto the image. We use binary search strategy to reduce the searching window (start line T_S and ending line T_E) gradually to find the best scan line *T*. Taking forward-looking image as an example, the search and projection steps are as follows.

Step 1. The initial searching window is set to be $T_S^{(0)}$ =1, $T_E^{(0)}$ =N, $T^{(0)}$ =*Round((N+1)/2)*, where N is the number of lines.

Step 2. Calculate the x coordinate in the forward-looking image using collinearity equation (11) and the EOPs of T^0.

$$x = -f\frac{a_1(X-X_i)+b_1(Y-Y_i)+c_1(Z-Z_i)}{a_3(X-X_i)+b_3(Y-Y_i)+c_3(Z-Z_i)} \qquad (11)$$

If $dx=x-x_{forward}<0$, set $T_S^{(1)}=T_S^{(0)}$, $T_E^{(1)}=T^{(0)}$, otherwise, set $T_S^{(1)}=T^{(0)}$, $T_E^{(1)}=T_E^{(0)}$. Calculate $T^{(1)}=Round((T_S^{(1)}+T_E^{(1)})/2)$. Iterate until $\left|T_S^{(i)}-T_E^{(i)}\right|$ is less than a threshold (e.g., 10 lines).

Step 3. Calculate the projected x values of the LAM point using the EOPs of each scan line in the window from $T_S^{(i)}$ to $T_E^{(i)}$ and compare with the ideal value $x_{forward}$. Take the line with the minimum absolute value of dx as the best line T_{min}.

Step 4. Project the LAM point using the EOPs of T_{min}. Repeat the process for all LAM points.

5. EXPERIMENTAL RESULTS

The developed method is tested using CE-1 stereo images of a 61km by 120 km area and 620 LAM points of 11orbits. The area has an elevation range from -2759.8 m to 719.2 m, referencing to the mean radius of 1737.4 km.

First, we project the LAM points onto the forward-, nadir-, and backward-looking images using the EOPs from 3rd polynomial fitting of trajectory and pointing data. Figure 7 shows a small portion of LAM points overlaid on the forward- and backward-looking images respectively. As can be seen from this figure, the projected LAM points are different from their true homologous points, showing that the two datasets are not very consistent.

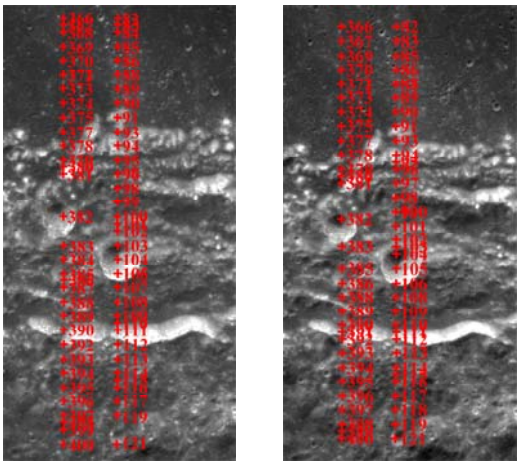

(a) Forward-looking image (b) Backward-looking image
Figure 7. LAM points overlaid on CCD stereo images

A 500 m resolution DEM is generated from the forward- and backward-looking images automatically. Figures 8 and 9 show 3D views of the CCD DEM and the LAM points before and after the co-registration respectively. Apparently, distances between LAM points and the CCD DEM have been reduced after the co-registration.

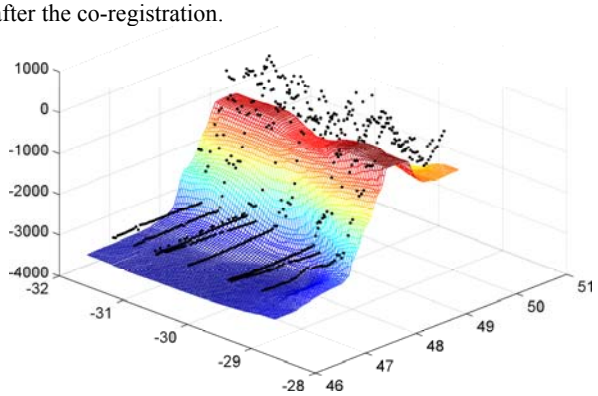

Figure 8. DEM and LAM point cloud before co-registration

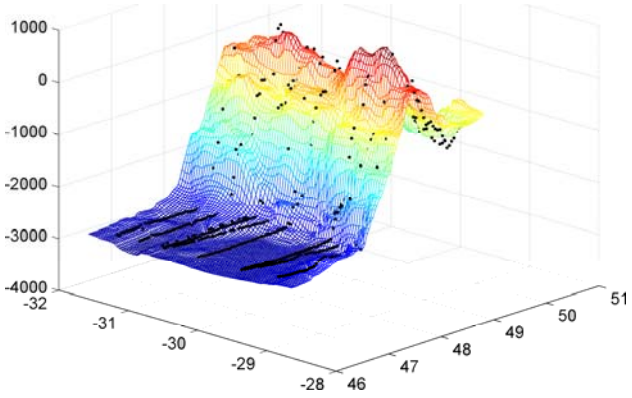

Figure 9. DEM and LAM point cloud after co-registration

We use the following two methods to evaluate the co-registration accuracy. (1) Taking the projected points in the nadir-looking image as base points, calculate the discrepancies between their homologous points (from image matching) and the projected positions of the LAM points in the forward- and backward-looking images respectively to depict the inconsistencies between the imagery and LAM data. (2) Re-calculate the 3D positions of LAM points from the projected image points in the stereo images using space intersection, and compare with the known LAM point coordinates.

Table 2 lists the discrepancies in image space before and after the co-registration of the CCD DEM and the LAM data. We can observe that the mean differences in the flight direction (row) have been reduced from over two pixels to sub-pixel level, while the differences in the cross-track direction and the RMSEs remain about the same. This indicates that the co-registration has effectively eliminated the systematic error in the flight direction. We can also observe that the discrepancies are generally in opposite directions in the forward- and backward-looking images.

		Forward (pixel)		Backward (pixel)	
		column	row	column	row
Before co-registration	mean	1.60	2.25	-1.37	-2.59
	RMSE	0.42	0.61	0.45	0.55
After co-registration	Mean	1.58	0.21	-1.38	-0.58
	RMSE	0.41	0.63	0.45	0.56

Table 2. Co-registration accuracy in image space

Table 3 lists the statistics of position differences in object space. The mean differences are reduced from several hundred meters to less than 20 meters. The RMSEs of the differences are only slightly reduced.

		ΔX(m)	ΔY(m)	ΔZ(m)
Before co-registration	Mean	400.387	-227.359	492.835
	RMSE	333.970	295.564	325.414
After co-registration	Mean	10.593	1.625	-17.526
	RMSE	305.859	291.513	298.568

Table 3. Co-registration accuracy in object space

Overall, the mean differences between the measurements from the CCD stereo images and the LAM data have been significantly reduced in both image and object space, which demonstrates the effectiveness of the proposed co-registration method. The RMSEs of the 3D discrepancies between the stereo images and the LAM data seem relatively large (about 300 m in X, Y and Z directions). Since no crossover correction has been applied to the LAM points, these discrepancies may partially attribute to the internal inconsistencies among the LAM points of different orbits. We expect to further improve the co-registration results after the crossover analysis of LAM data is performed.

6. CONCLUSIONS

It is necessary to register the stereo images and the LAM data of CE-1 for high accuracy and consistent mapping of the lunar surface. This will be more demanding when China's next lunar probe CE-2 acquires high-resolution stereo images for landing site characterization and preparation for soft landing. A method for co-registration of CE-1 stereo images and LAM data based on 3D surface matching was proposed and tested in this paper. The experimental results are promising. Further study incorporating crossover analysis of LAM data and more experiments will be performed.

ACKNOWLEDGEMENT

Funding of this research by National High Technology Research and Development Program of China (2009AA12z310) and National Natural Science Foundation of China (40871202) is acknowledged. We thank the National Astronomical Observatories of Chinese Academy of Sciences for providing the experimental data.

REFERENCES

Arun, K., T. Huang, S. Blostein, 1987. Least Square Fitting of Two 3-d Point Sets. *IEEE Transactions on Pattern Analysis and Machine Intelligence*, 9(5), pp. 698-700.

Besl, P., N. McKay, 1992. A Method for Registration of 3-d Shapes. *IEEE Transactions on Pattern Analysis and Machine Intelligence*, 14(2), pp. 239-256.

Du, G., 2009. China's lunar probe Chang'e-1 impacts moon. http://news.xinhuanet.com/english/2009-03/01/content_10923205.htm (accessed 1 sep. 2010)

Li, R., K. Di, A.B. Howard, L.H. Matthies, J. Wang, and S. Agarwal, 2007. Rock modeling and matching for autonomous long-range Mars rover localization, *Journal of Field Robotics*, 24(3), pp. 187-203.

Li, C., J. Liu, X. Ren, L. Mou, Y. Zou, H. Zhang, C. L, J. Liu, W. Zuo, Y. Su, W. Wen, W. Wen, B. Zhao, J. Yang, X. Zou, M. Wang, C. Xu, D. Kong, X. Wang, F. Wang, L. Geng, Z. Zhang, L. Zheng, X. Zhu, J. Li, 2010a. The Global Image of the Moon

by The Chang'E-1: Data Processing and Lunar Cartography. *Sci China Earth Sci*, 53(8), pp. 1091-1102, doi: 10.1007/s11430-010-4016-x.

Li, C., X. Ren, J. Liu, X. Zou, L. Mou, J. Wang, R. Shu, Y. Zou, H. Zhang, C, Lv, J. Liu, W. Zuo, Y. Su, W. Wen, W. Bian, M. Wang, C. Xu, D. Kong, X. Wang, F. Wang, L. Geng, Z. Zhang, L. Zheng, X. Zhu, J. Li, 2010b. Laser Altimetry Data of Chang'E-1 and the Global Lunar DEM model. *Sci China Earth Sci (in Chinese)*, 40(3), pp. 281-293, doi: 10.1007/s11430-010-0054-7.

Ping, J., Q. Huang, J. Yan, J. Cao, G. Tang, R. Shu, 2009. Lunar Topographic Model CLTM-s01 from Chang'E-1 Laser Altimeter. *Sci China Ser G-Phys Mech Astron*, 52(7), pp. 1105–1114.

Shan, J., J. Yoon, D. Lee, R. Kirk, G. Neumann, C. Acton, 2005. Photogrammetric Analysis of the Mars Global Surveyor Mapping Data. *Photogrammetric Engineering and Remote Sensing,* 71(1), pp. 97-108.

Sun, H., S. Dai, J. Yang, J. Wu and J. Jiang, 2005. Scientific objectives and payloads of Chang'E-1 lunar satellite. *Journal of Earth System Science,* 114, pp. 789–794. doi:10.1007/BF02715964.

Yoon, J., J. Shan, 2005. Combined Adjustment of MOC Stereo Imagey and MOLA Altimetry Data. *Photogrammetric Engineering and Remote Sensing,* 71(10), pp. 1179-1186.